JOURNAL OF GUIDANCE, CONTROL, AND DYNAMICS
Vol. 24, No. 4, July–August 2001

New Modeling and Control Design Techniques for Smart Deformable Aircraft Structures

Seung-Keon Kwak* and Rama K. Yedavalli†
The Ohio State University, Columbus, Ohio 43210-1276

A new modeling and control design specifically tailored to smart aeroelastic systems is presented. The control problem is to achieve a roll maneuver with a desired roll rate using a piezoelectric material laminated flexible wing subject to aerodynamic field. This multidisciplinary system of an elastic structure with piezoelectric actuating and sensing under external aerodynamic load is modeled with an integrated finite element method. The deformed structure for obtaining the specific roll rate is made up of new mass and stiffness matrices, which are functions of the steady-state input electric potential to piezoelectric actuators. The resulting model in the generalized coordinates, which has a mass matrix, a nonsymmetric aerodynamic damping matrix, and a nonsymmetric stiffness matrix (due to aerodynamic stiffness), is then transformed to real but nonorthogonal modal coordinates and a reduced-order model is developed. A new control design algorithm based on reciprocal state-space framework is introduced to achieve the desired roll rate and to dissipate vibrations by applying acceleration feedback.

Nomenclature

A	=	system matrix in state-space framework
B	=	input distribution matrix in state-space framework
$[B]$	=	differentiated shape functions
$\boldsymbol{B}$	=	actuator distribution matrix
C	=	damping matrix
C_A	=	aerodynamic damping matrix
C_{A_d}	=	aerodynamic damping matrix in deformed structure
C_L	=	lift coefficient
C_χ	=	modal damping matrix
$\boldsymbol{C}$	=	output matrix in state-space framework
c	=	airfoil chord length
$[c]$	=	structural stiffness
$[\bar{c}]$	=	transformed structural stiffness
D	=	electrical displacement
E	=	electric field
$[e]$	=	piezoelectric constant matrix
$[\bar{e}]$	=	transformed piezoelectric constant matrix
F	=	forcing function
f	=	external forcing function
G	=	system matrix in reciprocal state-space framework
G_c	=	closed-loop system matrix in reciprocal state-space framework
g	=	$\lambda(M^2-2)/U_a(M^2-1)$
H	=	input distribution matrix in reciprocal state-space framework
I	=	angular moment of inertia
J	=	Jacobian (structure)
J_a	=	Jacobian (aerodynamic)
J_d	=	Jacobian (deformed)
$\boldsymbol{J}$	=	performance index
K	=	stiffness matrix
$\boldsymbol{K}$	=	control gain
K_A	=	aerodynamic stiffness matrix
K_q	=	structural stiffness matrix
$K_{q\phi}$	=	piezoelectric coupling matrix
$K_{\phi\phi}$	=	dielectric stiffness matrix
L	=	lift
$[L]$	=	differential operator
l	=	length of wing
M	=	mass matrix
$\boldsymbol{M}$	=	Mach number
M_R	=	rolling moment
m	=	mass of wing
N	=	structural shape function
P	=	roll rate
Q	=	surface charge
$\boldsymbol{Q}$	=	weighting matrix in linear quadratic regulator (LQR) framework
q	=	generalized coordinates
$\boldsymbol{q}$	=	$\rho_a U_a^2/2$
$\boldsymbol{R}$	=	weighting matrix in LQR framework
S	=	strain vector
$\boldsymbol{S}$	=	optimal parameter
T	=	stress vector
$[T]$	=	transformation matrix
t	=	time coordinate
$\boldsymbol{t}$	=	surface traction
U_∞	=	air velocity
u, v, w	=	displacements
$\boldsymbol{u}$	=	displacement vector
$\boldsymbol{u}$	=	input vector in state-space framework
V	=	voltage
X	=	structural coordinates
x, y, z	=	structural coordinates
x', y', z'	=	principal axes
$\boldsymbol{x}$	=	state vector
$\boldsymbol{y}$	=	output vector in state-space framework
α	=	angle of attack
β	=	transformed coordinates
Γ	=	desired roll angle change
γ	=	shear strain
Δp	=	aerodynamic pressure difference
δ	=	variational operator
δT	=	first variation of kinetic energy
δU	=	first variation of potential energy
δW	=	first variation of work done by external force
$[\varepsilon]$	=	dielectric matrix
Θ	=	modified shape function
θ	=	skew angle
Λ	=	frequency matrix
Λ_i	=	frequency
λ	=	$2q/\sqrt{(M^2-1)}$
ξ, η, ζ	=	element local coordinates
ρ_a	=	air density
ϕ	=	roll angle

Received 20 October 1999; revision received 2 November 2000; accepted for publication 9 November 2000. Copyright © 2001 by the American Institute of Aeronautics and Astronautics, Inc. All rights reserved.

*Visiting Scholar, Department of Mechanical Engineering; kwak.21@osu.edu. Member AIAA.

†Professor, Department of Aerospace Engineering, Applied Mechanics and Aviation; yedavalli.1@osu.edu. Associate Fellow AIAA.

φ = generalized electric potential
χ = modal coordinates
Ψ = electric potential

Subscripts

a = air
d = deformed coordinates
E = electrical
i = node number
q = structural
r = roll
s = strain
t = stress
tw = twisting
x, y, z = structural coordinates

I. Introduction

IN nature, birds change their wing shapes to achieve proper flight performance. Humans have long pursued the dream of achieving birdlike flight performance. Efforts in that direction led to the development of rigid control surfaces such as an elevator, ailerons, a rudder, and flaps for conventional aircraft. However, these efforts were only adequate for limited flight envelopes and maneuvers although many modern fighter aircrafts are required to possess rapid maneuverability at various speeds and altitudes. For example, if one attempts to accomplish this rapid maneuver for the aircrafts with traditional control surfaces, many difficulties arise. One of them is the roll reversal phenomenon and the other is the vibration problem.

Aircraft's wings are deformed significantly due to high dynamic pressure during a swift roll motion. This deformation causes the roll reversal phenomenon.[1] In addition, structural vibrations of an aircraft, however, can cause discomfort and long-term component failure. This issue is compounded by space and weight limitations that reduce the effectiveness of active and passive controls. A properly deformable wing structure[2] is expected to enable the aircraft to have faster and gentler maneuverability as well as more efficient and safer performance than the traditional aircrafts. One way to achieve this goal, in an efficient manner, is to use piezoelectric components. Piezoelectric sensors and actuators are good candidates for active vibration and shape control in the aircraft structures because of their light weight, small volume, and various shapes. Numerous studies[3–7] have shown the utility of piezoelectric materials in structural vibration and noise control in aircraft.

In recent years, therefore, design and control of a deformable wing based on smart structure actuation and sensing has become an active topic of research in the aerospace community. Federal research laboratories such as Wright Laboratory and the Defence Advanced Research Projects Agency and industries such as Northrop Grumman Corporation are actively engaged in research and development of this challenging multidisciplinary area (elastic structures, smart materials, external aerodynamic pressure, flight mechanics, and control) with extensive applications.[8,9]

Most of the previous modeling and control design research in this multidisciplinary area is confined to integration of any two subdisciplines such as structures and control, control and smart materials, and structures and smart materials. Recently, attempts at the full-integrated problem of incorporating all five subdisciplines, namely, structures, aerodynamics, smart materials, flight mechanics, and control system design, are reported in Refs. 10 and 11. This type of pure and straightforward integration of these five disciplines is realized to be a complicated task requiring expertise in all of these disciplines.

In this paper, efforts are undertaken to model and control a flexible wing structure embedded with piezoelectric actuators. A desired roll rate is achieved by actively deforming the wing. Typically, the motion of the multidisciplinary flexible aircraft structures[3,4,12] can be expressed in the form of multivariable linear ordinary second-order differential equations in the configuration or generalized coordinates. In this study, the multidisciplinary flexible aircraft structural system is formed with a symmetric positive definite mass matrix but a nonsymmetric and indefinite damping (which includes aerodynamic damping) and stiffness (which includes aerodynamic and piezoelectric material stiffness in addition to the standard structural stiffness) matrices. To have constant roll rate and to dissipate vibrations by applying acceleration feedback, a new framework called reciprocal state space[3,13] is used for control design purposes. This new modeling and control design methodology is illustrated with the help of an example.

II. Integrated Modeling for Smart Flexible Deformable Wings

The equations of motion for multidisciplinary flexible aircraft structural systems, in general, have been formulated in the orthogonal coordinates for pure structural dynamics.[14] The aerodynamic pressure distribution to achieve roll motions, then, is assumed to be known along these modal coordinates. In this research, attempts are made to obtain a more generic modeling procedure that is applicable not only to the present problem of roll maneuvers but also to the future applications involving pitch, roll, and yaw maneuvers. With this in mind, it is realized that the equations of motion for the multidisciplinary aeroelastic system can be developed easier in the generalized coordinates than in the orthogonal modal coordinates. The elastic structure, piezoelectric coupling, aerodynamic pressure distribution, flight mechanics, and control design are simultaneously considered in the direct generalized coordinates, and then the complete model is transformed to generalized (possibly nonorthogonal) modal coordinates. A finite element modeling procedure is applied to develop the complete model of this multidisciplinary system. This is described in the next section.

A. Finite Element Modeling of a Deformable Wing

The constitutive equations for a piezoelectric material are expressed as[15]

$$T = [c]S - [e]^T E \tag{1}$$

$$D = [e]S + [\varepsilon]E \tag{2}$$

Accordingly, $[c]$, $[e]$, and $[\varepsilon]$ are given by

$$[c] = \begin{bmatrix} C_{11} & C_{12} & C_{13} & 0 & 0 & 0 \\ C_{21} & C_{22} & C_{23} & 0 & 0 & 0 \\ C_{31} & C_{32} & C_{33} & 0 & 0 & 0 \\ 0 & 0 & 0 & C_{44} & 0 & 0 \\ 0 & 0 & 0 & 0 & C_{44} & 0 \\ 0 & 0 & 0 & 0 & 0 & C_{44} \end{bmatrix} \tag{3}$$

$$[e] = \begin{bmatrix} 0 & 0 & 0 & 0 & e_{15} & 0 \\ 0 & 0 & 0 & e_{24} & 0 & 0 \\ e_{31} & e_{32} & e_{33} & 0 & 0 & 0 \end{bmatrix} \tag{4}$$

$$[\varepsilon] = \begin{bmatrix} \varepsilon_{11} & 0 & 0 \\ 0 & \varepsilon_{11} & 0 \\ 0 & 0 & \varepsilon_{33} \end{bmatrix} \tag{5}$$

To generate the finite element formulation of a flexible wing, an eight-node coupled brick element is selected as shown in Fig. 1. The shape functions of the elements are expressed as

$$N_i = \tfrac{1}{8}(1 + \xi\xi_i)(1 + \eta\eta_i)(1 + \zeta\zeta_i), \qquad i = 1, \ldots, 8 \tag{6}$$

Each node of the element has four degrees of freedom, which are spatial displacements u, v, and w and electric potential φ. These displacements and electric potential are coupled to each other according to the constitutive equations (1) and (2). The displacement fields with the shape functions in the finite element model are expressed as

$$\boldsymbol{u} = \lfloor N_q \rfloor q \tag{7}$$

$$\Psi = [N_E]\varphi \tag{8}$$

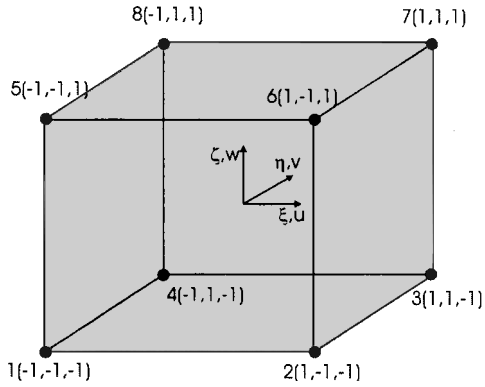

Fig. 1 Coupled eight nodes, three-dimensional solid.

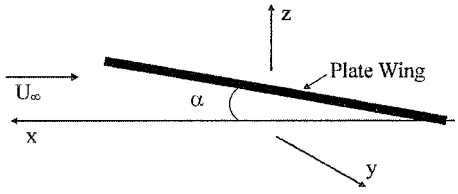

Fig. 2a Angle of attack.

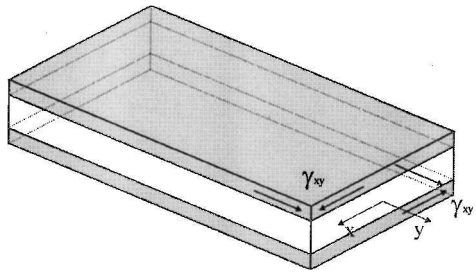

Fig. 2b Shear strains.

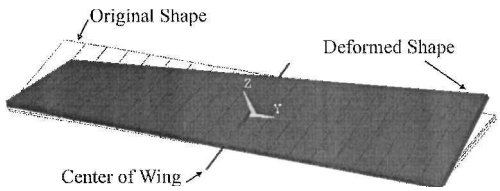

Fig. 3 Finite element analysis of a twisting wing.

where $\lfloor N_q \rfloor$ and $[N_E]$ are the shape functions in the q and φ coordinates. Then the strain and electric fields are written as

$$S = \lfloor L_q \rfloor \lfloor N_q \rfloor q = \lfloor B_q \rfloor q \tag{9}$$

$$E = [L_E][N_E]\varphi = \lfloor B_\varphi \rfloor \varphi \tag{10}$$

where $\lfloor L_q \rfloor$ and $[L_E]$ are differential operators.

B. Torsional Motion of Piezoelectric Continua

Recall that lift forces vary as the angles of attack α of a wing, which can be changed by the twisting motion of the wing. It is clear that one needs to impart twisting motion to the wing to generate the required moments for various flight maneuvers such as roll. Figures 2a and 3 show the angle of attack and twisting motion of a wing, respectively.

The twisting motion of a plate can be achieved by producing a pair of shear strains γ_{xy} in opposite directions as shown in Fig. 2b. In this study, the directional attachment technique of the polyvinylidene fluoride (PVDF) actuators[16–18] is employed to achieve twisting motion of the wing. As shown in Fig. 4, two PVDF layers, bottom and upper layers, are attached to a plate with opposite skew angles θ and $-\theta$ to generate the torque on the plate. The relations between the

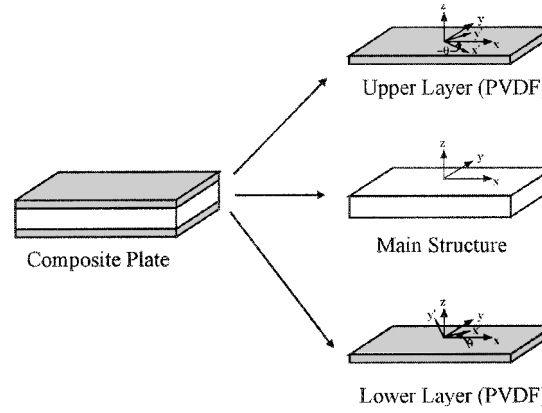

Fig. 4 Skew angles.

principal axes (x', y', z') and reference axes (x, y, z) are expressed as

$$T' = [T_t]T \tag{11}$$

$$S' = [T_s]S \tag{12}$$

where $[T_t]$ and $[T_s]$ are coordinate transformation matrices shown in Ref. 19. Now, Eqs. (1) and (2) can be expressed as

$$T = [\bar{c}]S - [\bar{e}]^T E \tag{13}$$

$$D = [\bar{e}]S + [\varepsilon]E \tag{14}$$

where

$$[\bar{c}] = [T_t]^{-1}[c][T_s] \tag{15}$$

$$[\bar{e}] = [e]T_s \tag{16}$$

It is shown in Ref. 18 that the transformed piezoelectric matrix $[\bar{e}]$ has a nonzero e_{36} entry. The importance of this entry is that the torsional motion can be produced by this coefficient. The maximum shear strain γ_{xy} can be obtained when the skew angles are $\pi/4$ (Ref. 18).

C. Modeling of Aerodynamic Pressure Distribution

The modeling of aerodynamic pressure distribution on the flexible wing structure is considered. According to piston theory,[20,21] the aerodynamic pressure on the surface of a wing for a high Mach number ($M > 1.6$) is expressed as

$$\Delta p = -\left[\lambda\left(\frac{\partial w}{\partial x}\right) + g\left(\frac{\partial w}{\partial t}\right)\right] \tag{17}$$

where w is the nodal displacement in z direction. The constants λ and g are given by

$$\lambda = 2q\Big/\sqrt{M^2 - 1} \tag{18}$$

$$g = (\lambda/U_\infty)[(M^2 - 2)/(M^2 - 1)] \tag{19}$$

$$q = \tfrac{1}{2}\rho_a U_\infty^2 \tag{20}$$

where U_∞ is air velocity. Figure 5 shows a 32-degrees-of-freedom brick element with aerodynamic loads. According to Eq. (18), these loads are changed by the vertical displacements of nodes. It is assumed that the loads change along the x and ξ coordinates and the pressure difference between upper and lower surfaces of the wing act on the upper surface as shown in Fig. 5. By substituting Eq. (7) into Eq. (17), we obtain

$$\Delta p = -\lambda[B_a]q - g[N_a]\dot{q} \tag{21}$$

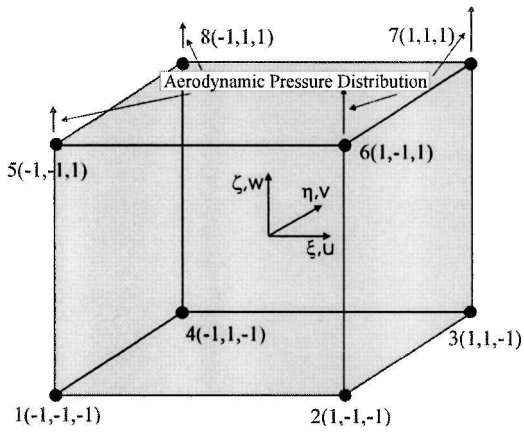

Fig. 5 Coupled eight nodes, three-dimensional solid with aerodynamic loads.

where $[N_a]$ and $[B_a]$ are given as

$$[N_a] = \begin{bmatrix} 0 & 0 & 0 & 0 & 0 & 0 & \cdots & 0 & 0 & 0 \\ 0 & 0 & 0 & 0 & 0 & 0 & \cdots & 0 & 0 & 0 \\ 0 & 0 & N_{1,\zeta=1} & 0 & 0 & N_{2,\zeta=1} & \cdots & 0 & 0 & N_{8,\zeta=1} \end{bmatrix} \tag{22}$$

$$[B_a] = \begin{bmatrix} 0 & 0 & 0 & 0 & 0 & 0 & \cdots & 0 & 0 & 0 \\ 0 & 0 & 0 & 0 & 0 & 0 & \cdots & 0 & 0 & 0 \\ 0 & 0 & \left.\dfrac{\partial N_1}{\partial \xi}\right|_{\zeta=1} & 0 & 0 & \left.\dfrac{\partial N_2}{\partial \xi}\right|_{\zeta=1} & \cdots & 0 & 0 & \left.\dfrac{\partial N_8}{\partial \xi}\right|_{\zeta=1} \end{bmatrix} \tag{23}$$

D. Equation of Motion via Hamilton's Principle

The equation of motion of the twisting wing can be derived from Hamilton's principle, which is expressed as

$$\int_{t_1}^{t_2} (\delta T - \delta U + \delta W)\,\mathrm{d}t = 0 \tag{24}$$

where δU is the first variation of total potential energy. The potential energy includes the conservative mechanical strain energy and the electrical energy. The energy terms δT, δU, and δw are expressed as[15,22,23]

$$\delta T = \int_v \rho \dot{\boldsymbol{u}}\,\delta\dot{\boldsymbol{u}}\,\mathrm{d}V \tag{25}$$

$$\delta U = \int_v \{\delta S^T[\bar{c}]S - \delta S^T[\bar{e}]^T E - \delta E^T[\bar{e}]S - \delta E^T[\varepsilon]E\}\,\mathrm{d}V \tag{26}$$

$$\delta W = \int_s \{\boldsymbol{t}\delta\boldsymbol{u} - Q\delta\varphi\}\,\mathrm{d}S \tag{27}$$

where ρ is the mass density. By substituting Eqs. (25–27) into Eq. (24), one gets

$$\int_v \{\delta S^T[\bar{c}]S - \delta S^T[\bar{e}]^T E - \delta E^T[\bar{e}]S - \delta E^T[\varepsilon]E + \rho\delta\dot{\boldsymbol{u}}^T\ddot{\boldsymbol{u}}\}\,\mathrm{d}V - \int_s \{\delta\boldsymbol{u}^T\boldsymbol{t} - Q\delta\varphi\}\,\mathrm{d}S = 0 \tag{28}$$

By substituting Eqs. (7–10) into Eq. (28), one can combine Hamilton's principle with the finite element method to obtain

$$\begin{aligned} \int_v \Big\{ & \delta q^T[B_q]^T[\bar{c}][B_q]q - \delta q^T[B_q]^T[\bar{e}]^T[B_\varphi]\varphi - \delta\varphi^T[B_\varphi]^T[\bar{e}][B_\varphi]q \\ & - \delta\varphi^T[B_\varphi]^T[\varepsilon][B_\varphi]\varphi + \rho\delta q^T[N_q]^T[N_q]\ddot{q}\Big\}\,\mathrm{d}V \\ & - \int_s \Big\{\delta q^T[N_q]^T_{\zeta=1}(-\lambda[B_a]q - g[N_a]\dot{q}) \\ & - \delta\varphi^T[N_E]^T Q\Big\}\,\mathrm{d}S = 0 \end{aligned} \tag{29}$$

Equation (29) can be reorganized as

$$\begin{aligned} \delta q^T \Bigg\{ & \int_v [B_q]^T[\bar{c}][B_q]\,\mathrm{d}V q + \int_v [B_q]^T[\bar{e}]^T[B_\varphi]\,\mathrm{d}V\varphi \\ & + \int_v \rho[N_q]^T[N_q]\,\mathrm{d}V\ddot{q} + \int_s g[N_q]^T_{\zeta=1}[N_a]\,\mathrm{d}S\dot{q} \\ & + \int_s \lambda[N_q]^T_{\zeta=1}[B_a]\,\mathrm{d}S q\Bigg\} + \delta\varphi^T\Bigg\{\int_v [B_\varphi]^T[\bar{e}][B_q]\,\mathrm{d}V q \\ & + \int_v [B_\varphi]^T[\varepsilon][B_\varphi]\,\mathrm{d}V\varphi - \int_s [N_E]^T Q\,\mathrm{d}S\Bigg\} = 0 \end{aligned} \tag{30}$$

From Eq. (30), the mass, stiffness, and damping matrices can be defined in the brick element local coordinates. These matrices are given by

$$M = \int_{-1}^{1}\int_{-1}^{1}\int_{-1}^{1} \rho[N_q]^T[N_q]|J|\,\mathrm{d}\xi\,\mathrm{d}\eta\,\mathrm{d}\zeta \tag{31}$$

$$C_A = \int_{-1}^{1}\int_{-1}^{1} g[N_q]^T_{\zeta=1}[N_a]|J_a|\,\mathrm{d}\xi\,\mathrm{d}\eta \tag{32}$$

$$K_q = \int_{-1}^{1}\int_{-1}^{1}\int_{-1}^{1} [B_q]^T[c][B_q]|J|\,\mathrm{d}\xi\,\mathrm{d}\eta\,\mathrm{d}\zeta \tag{33}$$

$$K_A = \int_{-1}^{1}\int_{-1}^{1} \lambda[N_q]^T_{\zeta=1}[B_a]|J_a|\,\mathrm{d}\xi\,\mathrm{d}\eta \tag{34}$$

$$K_{q\varphi} = \int_{-1}^{1}\int_{-1}^{1}\int_{-1}^{1} [B_q]^T[e]^T[B_\varphi]|J|\,\mathrm{d}\xi\,\mathrm{d}\eta\,\mathrm{d}\zeta \tag{35}$$

$$K_{\varphi q} = K_{q\varphi}^T \tag{36}$$

$$K_{\varphi\varphi} = \int_{-1}^{1}\int_{-1}^{1}\int_{-1}^{1} [B_\varphi]^T[\varepsilon][B_\varphi]|J|\,\mathrm{d}\xi\,\mathrm{d}\eta\,\mathrm{d}\zeta \tag{37}$$

and J and J_a are the Jacobian matrices:

$$J = \begin{bmatrix} \dfrac{\partial N_1}{\partial\xi} & \dfrac{\partial N_2}{\partial\xi} & \dfrac{\partial N_3}{\partial\xi} & \dfrac{\partial N_4}{\partial\xi} & \dfrac{\partial N_5}{\partial\xi} & \dfrac{\partial N_6}{\partial\xi} & \dfrac{\partial N_7}{\partial\xi} & \dfrac{\partial N_8}{\partial\xi} \\ \dfrac{\partial N_1}{\partial\eta} & \dfrac{\partial N_2}{\partial\eta} & \dfrac{\partial N_3}{\partial\eta} & \dfrac{\partial N_4}{\partial\eta} & \dfrac{\partial N_5}{\partial\eta} & \dfrac{\partial N_6}{\partial\eta} & \dfrac{\partial N_7}{\partial\eta} & \dfrac{\partial N_8}{\partial\eta} \\ \dfrac{\partial N_1}{\partial\zeta} & \dfrac{\partial N_2}{\partial\zeta} & \dfrac{\partial N_3}{\partial\zeta} & \dfrac{\partial N_4}{\partial\zeta} & \dfrac{\partial N_5}{\partial\zeta} & \dfrac{\partial N_6}{\partial\zeta} & \dfrac{\partial N_7}{\partial\zeta} & \dfrac{\partial N_8}{\partial\zeta} \end{bmatrix} \times \begin{bmatrix} x_1 & y_1 & z_1 \\ x_2 & y_2 & z_2 \\ x_3 & y_3 & z_3 \\ x_4 & y_4 & z_4 \\ x_5 & y_5 & z_5 \\ x_6 & y_6 & z_6 \\ x_7 & y_7 & z_7 \\ x_8 & y_8 & z_8 \end{bmatrix} \tag{38}$$

$$J_a = \begin{bmatrix} \dfrac{\partial N_1}{\partial \xi} & \dfrac{\partial N_2}{\partial \xi} & \dfrac{\partial N_3}{\partial \xi} & \dfrac{\partial N_4}{\partial \xi} \\ \dfrac{\partial N_1}{\partial \eta} & \dfrac{\partial N_2}{\partial \eta} & \dfrac{\partial N_3}{\partial \eta} & \dfrac{\partial N_4}{\partial \eta} \end{bmatrix} \begin{bmatrix} x_1 & y_1 \\ x_2 & y_2 \\ x_3 & y_3 \\ x_4 & y_4 \end{bmatrix} \tag{39}$$

According to Eq. (21), the aerodynamic loads are expressed in terms of the generalized coordinates. Moreover, in Eqs. (32) and (34), the loads are grouped as the stiffness and damping coefficient matrices of the system. These coefficients are labeled as the aerodynamic stiffness and damping matrices. When Eq. (30) is rewritten in a matrix form, the well-known matrix second-order system[24] can be obtained as

$$\begin{bmatrix} M & 0 \\ 0 & 0 \end{bmatrix} \begin{bmatrix} \ddot{q} \\ \ddot{\varphi} \end{bmatrix} + \begin{bmatrix} C_A & 0 \\ 0 & 0 \end{bmatrix} \begin{bmatrix} \dot{q} \\ \dot{\varphi} \end{bmatrix} + \begin{bmatrix} K_q + K_A & K_{q\varphi} \\ K_{\varphi q} & K_{\varphi\varphi} \end{bmatrix} \begin{bmatrix} q \\ \varphi \end{bmatrix} = \begin{bmatrix} 0 \\ Q \end{bmatrix} \tag{40}$$

III. Equation of Steady Roll

In this section, the roll maneuver with a constant roll rate is analyzed. In aerodynamic field, the roll motion can be achieved by twisting motion of an active deformable wing. The twisting motion is produced by the steady-state electric potential actuation through piezoelectric actuators. Because the model of the wing is expressed with nodal displacements and electric potentials, the angular displacement cannot be directly shown in generalized coordinates. In this study, therefore, the angular displacement of roll motion (Fig. 6) and its relationship to the input voltage are developed.

The roll equation of motion for the wing is obtained from the moment equilibrium equation:

$$I\ddot{\phi} = M_R \tag{41}$$

where ϕ and M_R are roll angle and rolling moment due to lift, respectively. The angular moment of inertia I is expressed as

$$I = \tfrac{1}{3}ml^2 \tag{42}$$

where l is a half length of the wing. The rolling moment due to lift M_R is expressed as

$$M_R = \int_0^l L(y)\,\mathrm{d}y \tag{43}$$

where $L(y)$ is lift force,

$$L(y) = qcC_L(y) \tag{44}$$

where $\boldsymbol{q} = (\rho U^2/2)$ and U are dynamic pressure and air velocity, respectively. The lift coefficient $C_L(y)$ can be expressed as a function of angle of attack α as

$$C_L(y) = \frac{\partial C_L(y)}{\partial \alpha}[\alpha_0(y) + \alpha_e(y)] = C_{L_0} + \frac{\partial C_L}{\partial \alpha}\alpha_e(y) \tag{45}$$

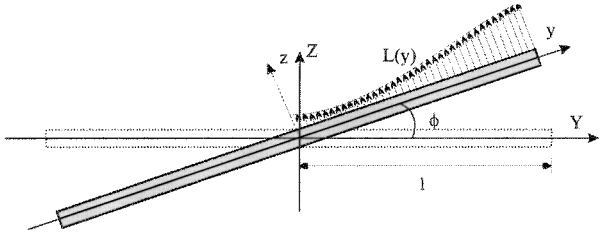

Fig. 6 Roll motion of wing.

where $\alpha_0(y)$ is angle of attack for zero lift and it is assumed that $\alpha_0(y)$ is zero. Note that, $\alpha_e(y)$ can be written as[25]

$$\alpha_e(y) = \alpha_{pz}(y) - Py/U \tag{46}$$

where $\alpha_{pz}(y)$ is the angle of attack produced by piezoelectric actuation and Py/U is the induced angle of attack due to roll rate P (Ref. 25). When Eq. (46) is substituted into Eq. (45), the lift coefficient is written as

$$C_L(y) = C_{L\alpha}[\alpha_{pz}(y) - Py/U] \tag{47}$$

where $C_{L\alpha} = \partial C_L(y)/\partial\alpha$. When Eq. (47) is introduced into Eq. (45), the lift is expressed as

$$\begin{aligned} L(y) &= C_{L\alpha}\boldsymbol{q}c[\alpha_{pz}(y) - Py/U] \\ &= \left(C_{L\alpha}\rho cU^2/2\right)[\alpha_{pz}(y) - Py/U] \end{aligned} \tag{48}$$

Then, the rolling moment is obtained as

$$\begin{aligned} M_R &= \frac{C_{L\alpha}\rho cU^2}{2}\int_0^l \left[\alpha_{pz}(y) - \frac{Py}{U}\right]\mathrm{d}y \\ &= \frac{C_{L\alpha}\rho cU^2}{2}\left[-\frac{Pl^2}{2U} + \int_0^l \alpha_{pz}(y)\,\mathrm{d}y\right] \end{aligned} \tag{49}$$

When Eq. (49) is substituted into Eq. (41) and $P = \dot{\phi}$ is used, the equation of motion for the roll can be expressed as

$$\frac{1}{3}ml^2\ddot{\phi} + \frac{C_{L\alpha}\rho cUl^2}{4}\dot{\phi} = \frac{C_{L\alpha}\rho cU^2}{2}\int_0^l \alpha_{pz}(y)\,\mathrm{d}y \tag{50}$$

A finite element model analysis (Fig. 7) is applied to find the relationship between the angle of attack $\alpha_{pz}(y)$ and the nodal electric potential φ. For the purpose of modeling, it is assumed that chordwise segments of the wing remain rigid. Figure 8 shows the cross-sectional area and angle of attack α of the wing.

The angle α is the twisting angle due to the piezoelectric actuation in the element local coordinates. First, the angle of attack in the element coordinates, $\alpha_{pz}(\eta)$, has to be obtained. It is assumed that the angle α is constant through the chord line for small twist angles. The angle of attack is measured from the centerline of the cross section of the wing. In the element local coordinates, the angle α_{pz} is expressed as

$$\alpha_{pz}(\eta) = \left.\frac{\partial w}{\partial \xi}\right|_{\zeta = c_\zeta} \tag{51}$$

where c_ζ is the coordinate value for centerline of the cross-sectional area of the wing in the local coordinate. Finally, the angle α_{pz} is expressed in the generalized coordinates as

$$\alpha_{pz}(\eta) = [L_{\mathrm{tw}}]\lfloor N_q \rfloor q = [B_{\mathrm{tw}}]q \tag{52}$$

where

$$[L_{\mathrm{tw}}] = \begin{bmatrix} 0 & 0 & \left.\dfrac{\partial}{\partial \xi}\right|_{\zeta = c_\zeta} \end{bmatrix} \tag{53}$$

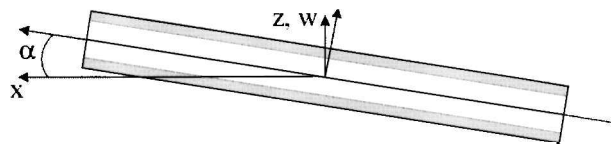

Fig. 8 Cross section of wing.

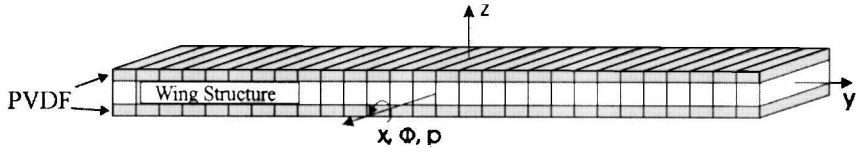

Fig. 7 Finite element model of wing plate with piezoelectric lamina.

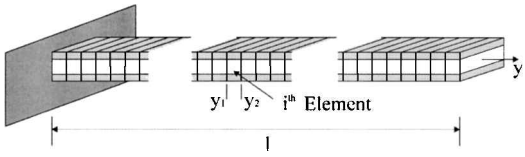

Fig. 9 Finite element model for wing.

$$[B_{\text{tw}}] =$$

$$\left[0 \quad 0 \quad \left.\frac{\partial N_1}{\partial \xi}\right|_{\zeta = c_\zeta} \quad 0 \quad 0 \quad \left.\frac{\partial N_2}{\partial \xi}\right|_{\zeta = c_\zeta} \quad \cdots \quad 0 \quad 0 \quad \left.\frac{\partial N_8}{\partial \xi}\right|_{\zeta = c_\zeta} \right] \tag{54}$$

$$q = [u_1 \quad v_1 \quad w_1 \quad u_2 \quad v_2 \quad w_2 \quad \cdots \quad u_8 \quad v_8 \quad w_8]^T \tag{55}$$

To build a full model, the angle of attack has to be integrated into the physical coordinates expressed as

$$\int_{y_1}^{y_2} \alpha_{pz}(y)\,\mathrm{d}y \tag{56}$$

where y_1 and y_2 are lower and upper bound for the jth element in the y coordinate as shown in Fig. 9. Because the twisting angle is constant throughout the chord line, ξ can be selected as zero. Then, the modified shape function Θ and y coordinate in the finite element are expressed as

$$\Theta_i = \tfrac{1}{8}(1 + \eta\eta_i)(1 + c_\zeta \zeta_i) \tag{57}$$

$$y = \sum_{i=1}^{8} \Theta_i y_i \tag{58}$$

From the chain rule,

$$\mathrm{d}y = \frac{\mathrm{d}y}{\mathrm{d}\eta}\,\mathrm{d}\eta \tag{59}$$

$$\frac{\mathrm{d}y}{\mathrm{d}\eta} = \sum_{i=1}^{8} \frac{\mathrm{d}\Theta_i}{\mathrm{d}\eta} y_i \tag{60}$$

The angle of attack for the jth structural element in the physical coordinate y is expressed as

$$A_j = \int_{y_1}^{y_2} \alpha_{pz}(y)\,\mathrm{d}y = \int_{-1}^{1} \alpha_{pz}(\eta) \sum_{i=1}^{8} \frac{\mathrm{d}\Theta_i}{\mathrm{d}\eta} y_{j_i}\,\mathrm{d}\eta$$

$$= \int_{-1}^{1} [B_{\text{tw}}] \sum_{i=1}^{8} \frac{\mathrm{d}\Theta_i}{\mathrm{d}\eta} y_{j_i}\,\mathrm{d}\eta q_j = [B_\alpha] J_{\alpha_j} q_j \tag{61}$$

where q_j, the generalized coordinates for jth element and $[B_\alpha]$ and J_{α_j}, are given as

$$[B_\alpha] = \left[0 \quad 0 \quad \int_{-1}^{1} \left.\frac{\partial N_1}{\partial \xi}\right|_{\zeta = c_\zeta} \mathrm{d}\eta \quad 0 \quad 0 \quad \int_{-1}^{1} \left.\frac{\partial N_2}{\partial \xi}\right|_{\zeta = c_\zeta} \mathrm{d}\eta \quad \cdots \quad 0 \quad 0 \quad \int_{-1}^{1} \left.\frac{\partial N_8}{\partial \xi}\right|_{\zeta = c_\zeta} \mathrm{d}\eta \right] \tag{62}$$

$$J_{\alpha_j} = \sum_{i=1}^{8} \frac{\mathrm{d}\Theta_i}{\mathrm{d}\eta} y_{j_i}\,\mathrm{d}\eta \tag{63}$$

Thus, the total integration of the angle of attack is written as

$$\int_0^l \alpha_{pz}(y)\,\mathrm{d}y = \sum_{j=1}^{p} A_j = [B_{\alpha q}] q \tag{64}$$

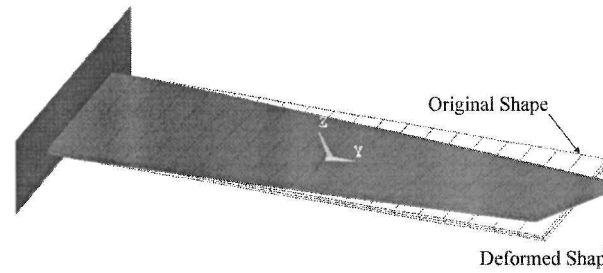

Fig. 10 Twisting motion of a cantilevered wing (finite element analysis).

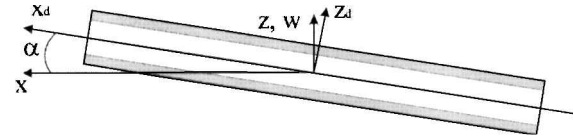

Fig. 11 Deformed coordinates.

where $\lfloor B_{\alpha q} \rfloor$ is the $(1 \times n)$ matrix, which is $[B_\alpha] \cdot J_{\alpha_j}$ for the corresponding nodal displacement q. The nodal displacement q due to the electric potential input φ can be obtained from the equation of motion of the cantilevered wing, which is expressed as

$$M_q \ddot{q} + K_q q = -K_{q\varphi} \varphi \tag{65}$$

Figure 10 shows the twisting motion of a cantilevered wing with voltage actuation. Because the twisting angle is the static deflection of the wing, Eq. (65) can be reduced to

$$K_q q = -K_{q\varphi} \varphi_r \tag{66}$$

where φ_r is the electric potential input for roll. Because the stiffness matrix of the cantilevered wing is nonsingular, the displacements are expressed as

$$q = -K_q^{-1} K_{q\varphi} \varphi_r \tag{67}$$

When Eqs. (50), (64), and (67) are combined, the equation of motion for roll motion with voltage actuation is expressed as

$$\tfrac{1}{3} m l^2 \ddot{\phi} + \left(C_{L_\alpha} \rho c U l^2 / 4\right) \dot{\phi} = -\left(C_{L_\alpha} \rho c U^2 / 2\right) B_{\alpha q} K_q^{-1} K_{q\varphi} \varphi_r \tag{68}$$

IV. Equation of Motion for Deformed Structure

A considerable amount of research exists on the vibration suppression of flexible structures.[4,7,26–28] In a roll maneuver with a flexible wing, a desired angle of attack should be maintained to achieve a desired roll rate. To maintain the desired angle of attack, the static deformation, twisting, of the wing need to be preserved. Therefore, a new equation of motion for the deformed structure is necessary to dissipate the vibration of the wing as well as to obtain the desired roll motion.

The finite element model based on the deformed coordinates, x_d, y_d, and z_d are defined as shown in Fig. 11. The displacement fields are then written as

$$\boldsymbol{u}_d = \lfloor N_q \rfloor q_d \tag{69}$$

$$\boldsymbol{\Psi}_d = \lfloor N_\varphi \rfloor \varphi_d \tag{70}$$

where

$$q_d = \begin{bmatrix} u_{d_1} & v_{d_1} & w_{d_1} & u_{d_2} & v_{d_2} & w_{d_2} & \cdots & u_{d_8} & v_{d_8} & w_{d_8} \end{bmatrix}^T \tag{71}$$

$$\varphi_d = \begin{bmatrix} V_{d_1} & V_{d_2} & \cdots & V_{d_8} \end{bmatrix}^T \tag{72}$$

The strain fields are expressed as

$$S_d = \lfloor B_q \rfloor q_d \tag{73}$$

$$E_d = \lfloor B_\varphi \rfloor \varphi_d \tag{74}$$

To obtain the equation of motion for the deformed structure, the following physical coordinates are used:

$$X_d = X + q_{\text{tw}} \tag{75}$$

where

$$X_d = \begin{bmatrix} x_{d_1} & y_{d_1} & z_{d_1} & x_{d_2} & y_{d_2} & z_{d_2} & \cdots & x_{d_8} & y_{d_8} & z_{d_8} \end{bmatrix}^T \tag{76}$$

$$X = [x_1 \quad y_1 \quad z_1 \quad x_2 \quad y_2 \quad z_2 \quad \cdots \quad x_8 \quad y_8 \quad z_8]^T \tag{77}$$

$$q_{\text{tw}} = \begin{bmatrix} q_{\text{tw}_1} & q_{\text{tw}_2} & \cdots & q_{\text{tw}_8} \end{bmatrix} \tag{78}$$

The static twisting displacement q_{tw} can be obtained from Eq. (67), which is expressed as

$$q_{\text{tw}} = -K_q^{-1} K_{q\varphi} \varphi_r \tag{79}$$

where φ_r is electric potential input for the desired roll. When Eq. (79) is substituted into Eq. (75), the deformed coordinates are expressed as

$$X_d = X - K_q^{-1} K_{q\varphi} \varphi_r \tag{80}$$

Finally, the equation of the motion for a deformed structure in the aerodynamic field is given by

$$\begin{bmatrix} M_d & 0 \\ 0 & 0 \end{bmatrix} \begin{bmatrix} \ddot{q}_d \\ \ddot{\varphi}_d \end{bmatrix} + \begin{bmatrix} C_{A_d} & 0 \\ 0 & 0 \end{bmatrix} \begin{bmatrix} \dot{q}_d \\ \dot{\varphi}_d \end{bmatrix} + \begin{bmatrix} K_d + K_{A_d} & K_{q\varphi_d} \\ K_{\varphi q_d} & K_{\varphi\varphi_d} \end{bmatrix} \begin{bmatrix} q_d \\ \varphi_d \end{bmatrix} = \begin{bmatrix} 0 \\ Q_d \end{bmatrix} \tag{81}$$

where

$$M_d = \int_{-1}^{1}\int_{-1}^{1}\int_{-1}^{1} \rho [N_q]^T [N_q] |J_d| \, \mathrm{d}\xi \, \mathrm{d}\eta \, \mathrm{d}\zeta \tag{82}$$

$$C_{A_d} = \int_{-1}^{1}\int_{-1}^{1} g [N_q]_{\zeta=1}^T [N_a] \left| J_{a_d} \right| \mathrm{d}\xi \, \mathrm{d}\eta \tag{83}$$

$$K_d = \int_{-1}^{1}\int_{-1}^{1}\int_{-1}^{1} [B_q]^T [c] [B_q] |J_d| \, \mathrm{d}\xi \, \mathrm{d}\eta \, \mathrm{d}\zeta \tag{84}$$

$$K_{A_d} = \int_{-1}^{1}\int_{-1}^{1} \lambda [N_q]_{\zeta=1}^T [N_a] \left| J_{a_d} \right| \mathrm{d}\xi \, \mathrm{d}\eta \tag{85}$$

$$K_{q\varphi_d} = \int_{-1}^{1}\int_{-1}^{1}\int_{-1}^{1} [B_q]^T [e]^T [B_\varphi] |J_d| \, \mathrm{d}\xi \, \mathrm{d}\eta \, \mathrm{d}\zeta \tag{86}$$

$$K_{\varphi q_d} = K_{q\varphi_d}^T \tag{87}$$

$$K_{\varphi\varphi_d} = \int_{-1}^{1}\int_{-1}^{1}\int_{-1}^{1} [B_\varphi]^T [\varepsilon] [B_\varphi] |J_d| \, \mathrm{d}\xi \, \mathrm{d}\eta \, \mathrm{d}\zeta \tag{88}$$

and J_d and J_{a_d} are the Jacobian matrices in the deformed coordinates:

$$J_d = \begin{bmatrix} \frac{\partial N_1}{\partial \xi} & \frac{\partial N_2}{\partial \xi} & \frac{\partial N_3}{\partial \xi} & \frac{\partial N_4}{\partial \xi} & \frac{\partial N_5}{\partial \xi} & \frac{\partial N_6}{\partial \xi} & \frac{\partial N_7}{\partial \xi} & \frac{\partial N_8}{\partial \xi} \\ \frac{\partial N_1}{\partial \eta} & \frac{\partial N_2}{\partial \eta} & \frac{\partial N_3}{\partial \eta} & \frac{\partial N_4}{\partial \eta} & \frac{\partial N_5}{\partial \eta} & \frac{\partial N_6}{\partial \eta} & \frac{\partial N_7}{\partial \eta} & \frac{\partial N_8}{\partial \eta} \\ \frac{\partial N_1}{\partial \zeta} & \frac{\partial N_2}{\partial \zeta} & \frac{\partial N_3}{\partial \zeta} & \frac{\partial N_4}{\partial \zeta} & \frac{\partial N_5}{\partial \zeta} & \frac{\partial N_6}{\partial \zeta} & \frac{\partial N_7}{\partial \zeta} & \frac{\partial N_8}{\partial \zeta} \end{bmatrix} \times \begin{bmatrix} x_{d_1} & y_{d_1} & z_d \\ x_{d_2} & y_{d_2} & z_{d_2} \\ x_{d_3} & y_{d_3} & z_{d_3} \\ x_{d_4} & y_{d_4} & z_{d_4} \\ x_{d_5} & y_{d_5} & z_{d_5} \\ x_{d_6} & y_{d_6} & z_{d_6} \\ x_{d_7} & y_{d_7} & d_7 \\ x_{d_8} & y_{d_8} & z_{d_8} \end{bmatrix} \tag{89}$$

$$J_a = \begin{bmatrix} \frac{\partial N_1}{\partial \xi} & \frac{\partial N_2}{\partial \xi} & \frac{\partial N_3}{\partial \xi} & \frac{\partial N_4}{\partial \xi} \\ \frac{\partial N_1}{\partial \eta} & \frac{\partial N_2}{\partial \eta} & \frac{\partial N_3}{\partial \eta} & \frac{\partial N_4}{\partial \eta} \end{bmatrix} \begin{bmatrix} x_{d_1} & y_{d_1} \\ x_{d_2} & y_{d_2} \\ x_{d_3} & y_{d_3} \\ x_{d_4} & y_{d_4} \end{bmatrix} \tag{90}$$

It is clear that the deformed structural mass, damping, and stiffness matrices are expressed as the functions of φ_r, which is input electric potential for the steady roll motion.

V. Model Reduction in Nonorthogonal Modal Coordinates

From Eq. (81), the equation of motion with voltage actuation is written as

$$M_d \ddot{q}_d + C_{A_d} \dot{q}_d + \left(K_d + K_{A_d}\right) q_d = -K_{q\varphi_d} \varphi_d \tag{91}$$

By premultiplying M^{-1} on both sides of Eq. (91), one gets

$$\ddot{q}_d + M_d^{-1} C_{A_d} \dot{q}_d + M_d^{-1} \left(K_d + K_{A_d}\right) q_d = -M_d^{-1} K_{q\varphi_d} \varphi_d \tag{92}$$

However, the model in this system is too large for a meaningful control system design. For this reason, a transformation to the nonorthogonal (but real) modal coordinates is carried out. The modal equation of motion of the system can be obtained with a similarity transformation that diagonalizes the integrated stiffness matrix.[29] Let

$$q_d = [T] \chi \tag{93}$$

where

$$[T] = [t_1 \quad t_2 \quad t_3 \quad \cdots \quad t_n], \qquad t_i : \text{ eigenvector of the system}$$

Then, Eq. (92) can be written as

$$\ddot{\chi} + C_\chi \dot{\chi} + \Lambda \chi = F_\chi \varphi_d \tag{94}$$

where

$$\chi = [\chi_1 \quad \chi_2 \quad \chi_3 \quad \cdots \quad \chi_n]^T \tag{95}$$

$$C_\chi = [T]^{-1} M_d^{-1} C_{A_d} [T] \tag{96}$$

$$\Lambda = [T]^{-1} M_d^{-1} \left(K_d + K_{A_d}\right) [T] = \text{diag}(\Lambda_1, \Lambda_2, \cdots \Lambda_n) \tag{97}$$

$$F_\chi = -[T]^{-1} M_d^{-1} K_{q\varphi_d} \tag{98}$$

and the eigenvalues Λ_i are complex numbers.

VI. Control Design Specifically Tailored to Smart Structural Systems

State-space representation is a useful tool to design controllers for linear systems, and many control design methods in the state-space framework are available to achieve stabilization and regulation of the state variables. However, for the particular problem at hand, to achieve a desired constant roll rate, the state-space based control design is cumbersome to use because the steady-state constant roll rate implies infinite roll displacements as time progresses. Therefore, the closed-loop system is considered unstable. To overcome this problem and still design a simple controller using available control system software for this desired roll rate achievement problem, a new framework called the reciprocal state-space framework is proposed.[13]

Note that the majority of the mechanical dynamic systems can be expressed in the form of a finite-dimensional, multivariable, matrix second-order (MSO) differential equation as [3,12,19,24,29–31]

$$M\ddot{q} + C\dot{q} + Kq = \boldsymbol{B}f \tag{99}$$

where $M_{n\times n}$, $C_{n\times n}$, and $K_{n\times n}$ are the mass, damping, and stiffness matrices, respectively. $\boldsymbol{B}_{n\times m}$ is an actuator distribution matrix and $q_{n\times 1}$ and $f_{m\times 1}$ are the generalized coordinate and the external forcing vector, respectively. Controllers and observers are designed, in general, after the MSO system is converted to this standard first-order state-space framework shown in Eq. (100). Full state feedback control in the state space is then written as

$$\begin{bmatrix}\dot{q}\\ \ddot{q}\end{bmatrix} = \begin{bmatrix}0 & I\\ -M^{-1}K & -M^{-1}C\end{bmatrix}\begin{bmatrix}q\\ \dot{q}\end{bmatrix} + \begin{bmatrix}0\\ M^{-1}B\end{bmatrix} f \tag{100}$$

$$\dot{\boldsymbol{x}} = A\boldsymbol{x} + B\boldsymbol{u} \tag{101}$$

$$\boldsymbol{u} = -\boldsymbol{K}\boldsymbol{x} \tag{102}$$

where $\boldsymbol{x} = [q \;\; \dot{q}]^T$ and $\boldsymbol{u} = f$. The closed-loop system is then given as

$$\dot{\boldsymbol{x}} = (A - B\boldsymbol{K})\boldsymbol{x} \tag{103}$$

According to Eqs. (100–103), the state variable $\boldsymbol{x}$ consists of displacement and velocity terms. Thus, it is not easy to implement a full state feedback control for structural systems in the state-space framework when we have acceleration measurements. In many structural applications, however, only acceleration measurements are available. To overcome this problem, a new control design technique named full state-derivative control based on the reciprocal state-space (RSS) framework[3,4,12,13] is introduced as shown in the following equations:

$$\boldsymbol{x} = G\dot{\boldsymbol{x}} + H\boldsymbol{u} \tag{104}$$

$$\boldsymbol{u} = -\boldsymbol{K}\dot{\boldsymbol{x}} \tag{105}$$

where

$$G = A^{-1} \tag{106}$$

$$H = -A^{-1}B \tag{107}$$

Note that the eigenvalues of the system matrix G in the RSS are the reciprocal of those in the standard state-space framework. Thus, the stability conditions for both the RSS and the standard state-space frameworks are the same. The closed-loop system in the RSS framework is given as

$$\boldsymbol{x} = (G - H\boldsymbol{K})\dot{\boldsymbol{x}} = G_c\dot{\boldsymbol{x}} \tag{108}$$

where G_c is a closed-loop system matrix. As shown in Eqs. (104), (105), and (108), the state derivative $\dot{\boldsymbol{x}}$, which has acceleration information, can be directly fed back in the RSS. Also, according to Refs. 3, 4, 12, and 13, most controller design techniques in the state-space framework like pole placement and linear quadratic regulator (LQR) can be directly applied to the RSS framework.

In the RSS framework the state derivatives, not the states themselves, are directly controlled. In other words, the state derivatives are minimized in an optimal fashion, when the RSS is applied to optimal control. The state-derivative performance index to be minimized is written as

$$\boldsymbol{J}_{\dot{x}} = \int_0^\infty \dot{\boldsymbol{x}}^T\dot{\boldsymbol{x}}\,\mathrm{d}t \tag{109}$$

By adding a control performance index, one gets the following nonstandard form:

$$\boldsymbol{J} = \int_0^\infty (\dot{\boldsymbol{x}}^T\boldsymbol{Q}\dot{\boldsymbol{x}} + \boldsymbol{u}^T\boldsymbol{R}\boldsymbol{u})\,\mathrm{d}t \tag{110}$$

This nonstandard performance index makes the state-derivative feedback controller design easy when compared to the standard output feedback in the state-space framework. For example, when the state derivatives are sensed and fed back in the state-space framework, the following output feedback relationship is obtained:

$$\boldsymbol{y} = \boldsymbol{C}\dot{\boldsymbol{x}} \tag{111}$$

$$\boldsymbol{u} = -\boldsymbol{K}\boldsymbol{y} \tag{112}$$

The control gain $\boldsymbol{K}$ can be found by using an optimal output feedback control design scheme. It is known that output feedback control is more complicated than state feedback control.[32,33] However, if we use the RSS framework, finding an optimal output feedback gain $\boldsymbol{K}$ becomes quite straightforward.[13] The control input in the RSS shown in Eq. (104) is given as

$$\boldsymbol{u} = \boldsymbol{K}\dot{\boldsymbol{x}} \tag{113}$$

In this framework, the closed-loop system becomes

$$\boldsymbol{x} = (G - H\boldsymbol{K})\dot{\boldsymbol{x}} = G_c\dot{\boldsymbol{x}} \tag{114}$$

Finding the $\boldsymbol{K}$ that minimizes $\boldsymbol{J}$ in this new system description is much easier because we can use the standard parameter optimization methodology to find the gains involved in the Lyapunov matrix. When Eq. (113) is substituted into Eq. (110), the performance index can be expressed as

$$J = \int_0^\infty [\dot{\boldsymbol{x}}^T\boldsymbol{Q}\dot{\boldsymbol{x}} + (\boldsymbol{K}\dot{\boldsymbol{x}})^T\boldsymbol{R}(\boldsymbol{K}\dot{\boldsymbol{x}})]\,\mathrm{d}t = \int_0^\infty \dot{\boldsymbol{x}}^T(\boldsymbol{Q} + \boldsymbol{K}^T\boldsymbol{R}\boldsymbol{K})\dot{\boldsymbol{x}}\,\mathrm{d}t \tag{115}$$

Suppose that we can find a constant, positive-semidefinite matrix $\boldsymbol{S}$ that satisfies[33,34]

$$\frac{\partial}{\partial t}(\boldsymbol{x}^T\boldsymbol{S}\boldsymbol{x}) = -\dot{\boldsymbol{x}}^T(\boldsymbol{Q} + \boldsymbol{K}^T\boldsymbol{R}\boldsymbol{K})\dot{\boldsymbol{x}} \tag{116}$$

Since $\boldsymbol{x} = G_c\dot{\boldsymbol{x}}$,

$$\frac{\partial}{\partial t}(\boldsymbol{x}^T\boldsymbol{S}\boldsymbol{x}) = \dot{\boldsymbol{x}}^T\left(\boldsymbol{S}G_c + G_c^T\boldsymbol{S}\right)\dot{\boldsymbol{x}} \tag{117}$$

Then, one may rewrite Eqs. (116) and (117) as

$$0 = \boldsymbol{S}G_c + G_c^T\boldsymbol{S} - \boldsymbol{K}^T\boldsymbol{R}\boldsymbol{K} + \boldsymbol{Q} \tag{118}$$

or

$$0 = \boldsymbol{S}G + G^T\boldsymbol{S} - \boldsymbol{S}H\boldsymbol{R}^{-1}H^T\boldsymbol{S} + \boldsymbol{Q} \tag{119}$$

This equation is the RSS version of well-known algebraic Ricatti equation. The corresponding feedback gain is expressed as

$$\boldsymbol{K} = \boldsymbol{R}^{-1}H^T\boldsymbol{S} \tag{120}$$

In this study, the RSS framework is employed to achieve the desired roll rate and to dissipate vibration of the wing. The state-space representation of the steady roll motion [Eq. (68)] is expressed as

$$\begin{bmatrix}\dot{\phi}\\ \ddot{\phi}\end{bmatrix} = \begin{bmatrix}0 & 1\\ 0 & -\dfrac{3C_{L_\alpha}\rho c U}{4m}\end{bmatrix}\begin{bmatrix}\phi\\ \dot{\phi}\end{bmatrix} + \begin{bmatrix}0\\ -\dfrac{3C_{L_\alpha}\rho c U^2}{2ml^2}[B_{\alpha q}][K_q]^{-1}[K_{q\varphi}]\end{bmatrix}\varphi_r \tag{121}$$

or

$$\dot{\boldsymbol{x}}_r = A_r \boldsymbol{x}_r + B_r \boldsymbol{u}_r \tag{122}$$

where $\boldsymbol{x}_r = [\phi \;\; \dot{\phi}]^T$ and subscript r is roll motion. The RSS representation of Eq. (122) is expressed as

$$\boldsymbol{x}_r = G_r \dot{\boldsymbol{x}}_r + H_r \boldsymbol{u}_r \tag{123}$$

$$\boldsymbol{u}_r = \boldsymbol{K}_r \dot{\boldsymbol{x}}_r \tag{124}$$

where

$$G_r = A_r^{-1} \tag{125}$$

$$H_r = -A_r^{-1} B_r \tag{126}$$

For a roll rate control, coordinates transformation are required in order to have a regulation problem. The coordinate transformations are expressed as

$$\dot{\beta} = \dot{\boldsymbol{x}}_r + P_d \tag{127}$$

$$\beta = \boldsymbol{x}_r + \Gamma \tag{128}$$

$$\Gamma = P_d t \tag{129}$$

where P_d and t are the desired roll rate and time, respectively. Then, Eqs. (123) and (124) are written as

$$\beta = G_r \dot{\beta} + H_r \boldsymbol{u}_r \tag{130}$$

$$\boldsymbol{u}_r = \boldsymbol{K}_r \dot{\beta} \tag{131}$$

From Eqs. (130) and (131), performance indices to be minimized are expressed as

$$\boldsymbol{J}_r = \int_0^\infty \left[\dot{\beta}^T \boldsymbol{Q}_r \dot{\beta} + \boldsymbol{u}_r^T \boldsymbol{R}_r \boldsymbol{u}_r\right] \mathrm{d}t \tag{132}$$

where $\boldsymbol{Q}_r$ is positive semidefinite and $\boldsymbol{R}_r$ is positive definite matrices. According to Refs. 32 and 34, the new LQR state-derivative feedback gain in the RSS is given as

$$\boldsymbol{K}_r = \boldsymbol{R}_r^{-1} H_r^T \boldsymbol{S}_r \tag{133}$$

The matrix $\boldsymbol{S}_r$ can be obtained from the associated algebraic matrix Riccati equation, which is expressed as

$$0 = \boldsymbol{S}_r G_r + G_r^T \boldsymbol{S}_r - \boldsymbol{S}_r H_r \boldsymbol{R}_r^{-1} H_r^T \boldsymbol{S}_r + \boldsymbol{Q}_r \tag{134}$$

Similarly, the vibratory equation of motion [Eq. (94)] for the flexible wing can be expressed in the state-space framework as

$$\begin{bmatrix}\dot{\chi}\\ \ddot{\chi}\end{bmatrix} = \begin{bmatrix}0 & I\\ -\Lambda & -C_\chi\end{bmatrix}\begin{bmatrix}\chi\\ \dot{\chi}\end{bmatrix} + \begin{bmatrix}0\\ F_\chi\end{bmatrix}\varphi_d \tag{135}$$

or

$$\dot{x} = Ax + B\boldsymbol{u} \tag{136}$$

where $x = [\chi \;\; \dot{\chi}]^T$. The RSS representation of Eqs. (135) and (136) are expressed as

$$\boldsymbol{x} = G\dot{\boldsymbol{x}} + H\boldsymbol{u} \tag{137}$$

$$\boldsymbol{u} = \boldsymbol{K}\dot{\boldsymbol{x}} \tag{138}$$

where

$$G = A^{-1} \tag{139}$$

$$H = -A^{-1}B \tag{140}$$

From Eqs. (137) and (138), performance indices to be minimized are expressed as

$$\boldsymbol{J} = \int_0^\infty [\dot{x}^T \boldsymbol{Q} \dot{x} + \boldsymbol{u}^T \boldsymbol{R} \boldsymbol{u}]\, \mathrm{d}t \tag{141}$$

where $\boldsymbol{Q}$ and $\boldsymbol{R}$ are positive semidefinite and positive definite matrices, respectively. The LQR state-derivative feedback gain in RSS is given as

$$\boldsymbol{K} = \boldsymbol{R}^{-1} H^T \boldsymbol{S} \tag{142}$$

The matrix $\boldsymbol{S}$ can be obtained from the associated algebraic matrix Riccati equation, which is expressed as

$$0 = \boldsymbol{S}G + G^T \boldsymbol{S} - \boldsymbol{S}H\boldsymbol{R}^{-1}H^T\boldsymbol{S} + \boldsymbol{Q} \tag{143}$$

VII. Illustrative Example for Roll and Vibration Control

A PVDF plate wing with 2 layers and 16 elements (Fig. 12) is selected for a control design whose objective is to achieve a desired constant roll rate. Each layer has an opposite skew angle to generate torques of the wing. One-half of the plate has eight, eight-node brick elements with the total number of nodes being 30. In other words, the system has 120 degrees of freedom, 90 for structural and 30 for electrical degrees of freedom. It is observed that the open-loop system is unstable.

Although a pure structural system is neutrally stable, in general, the structure in the aerodynamic field is no longer stable due to the presence of the nonconservative aerodynamic field, which brings forth some stiffness as well as damping. When the proposed control design technique is applied, the closed-loop system is not only stabilized but also a desired constant roll rate of 1.5 rad/s is achieved. The roll angles shown in Fig. 13 correspond to Fig. 14, which shows

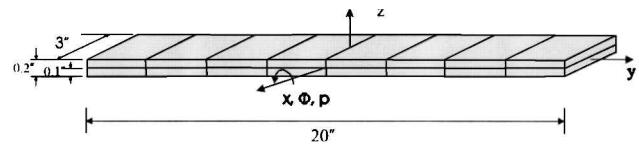

Fig. 12 Plate wing (PVDF).

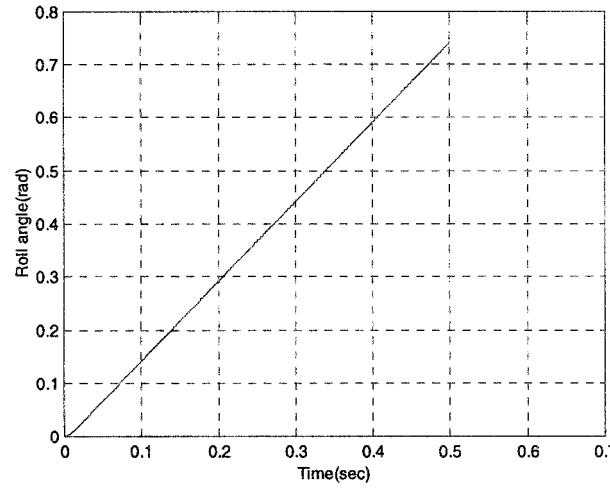

Fig. 13 Roll-angle responses (M = 2.0).

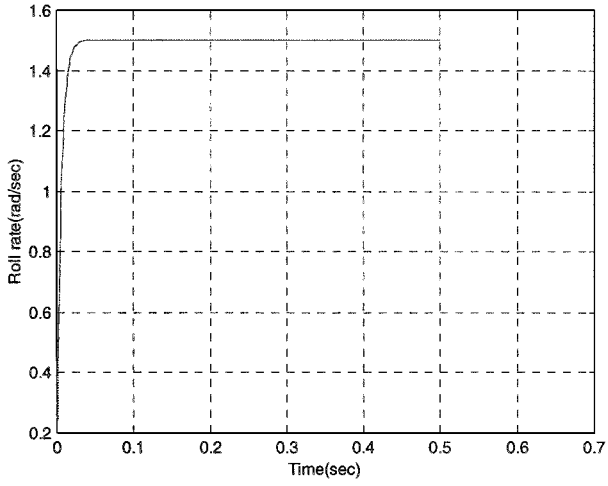

Fig. 14 Roll-rate responses (M = 2.0).

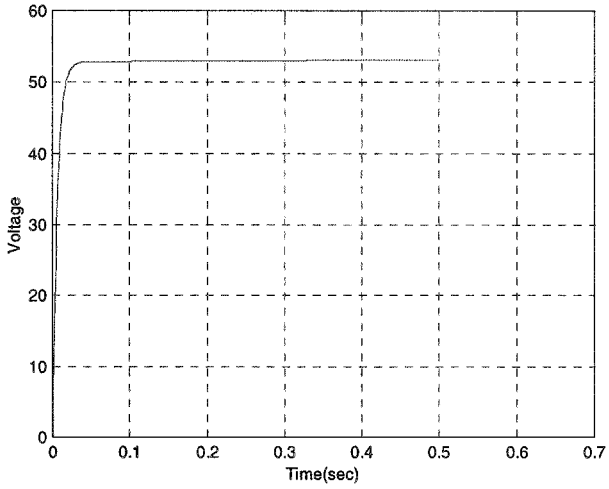

Fig. 15 Input voltages at node 2.

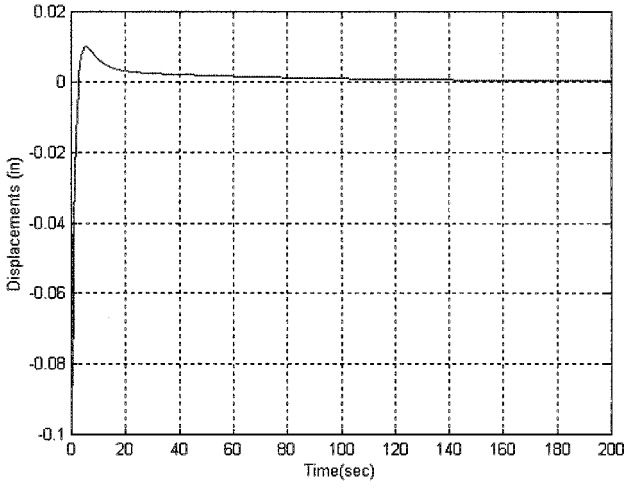

Fig. 16 Displacement responses (first flexible mode, M = 2.0).

the roll rate responses for a selected set of weighting matrices. From Fig. 14, it is clear that the desired roll velocity of 1.5 rad/s is achieved by the controller. The roll angle gradually increases as expected. Figure 15 shows the input voltage for the roll maneuver. The input voltage is used to build the deformed structure model. Figures 16 and 17 show the closed-loop responses for the first and second modes of vibrations of the wing plate that is deformed by the steady-state input voltage for the roll motion.

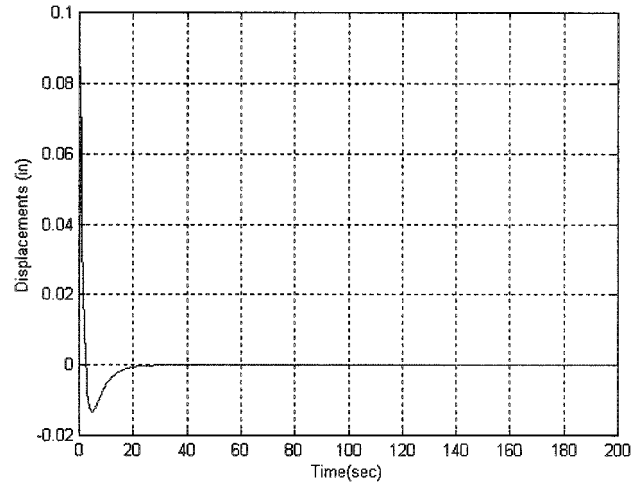

Fig. 17 Displacement responses (second flexible mode, M = 2.0).

VIII. Conclusions

In this research, an attempt is made to model the dynamics of a smart flexible wing involving the integration of five disciplines, namely, structures, aerodynamics, smart materials, control, and flight mechanics. The control objective is to sustain a roll maneuver with a desired roll rate and to suppress the flexible mode vibrations by actively deforming the wing. Modeling of this dynamics is done using finite element method in generalized coordinates. Because of the coupling between these subsystems, the resulting MSO system of equations consists of a symmetric positive definite mass matrix but a nonsymmetric and indefinite damping (which includes aerodynamic damping) and stiffness (which includes aerodynamic and piezoelectric material stiffness, in addition to the standard structural stiffness) matrices. The electric potential through the piezoelectric actuators serves as the control variables. The steady-state electric potential dependent mass, stiffness, and damping matrices are also determined to maintain the desired roll rate during the roll maneuver. For the vibration problem, the large model in generalized coordinates is then transformed to a set of nonorthogonal modal coordinates, and model reduction is carried out in these modal coordinates. The roll and vibration controls are designed in a new framework called reciprocal state space in which is implemented acceleration and velocity feedback control easily.

References

[1]Dowell, E. H., Sisto, F., Peters, D. A., Scanlan, R. H., Crawley, E. F., and Curtiss, H. C., Jr., *A Modern Course in Aeroelasticity*, 3rd ed., Kluwer Academic, Dordrecht, The Netherlands, 1995, pp. 34–41.

[2]Bonnema, K. L., et al., "AFTI/F-111 Mission Adaptive Wing Flight Research Program," AIAA Paper 88-2118, 1988.

[3]Kwak, S. K., and Yedavalli, R. K., "New Modeling and Control Design Techniques for Smart Deformable Aircraft Structures with Acceleration Feedback," *AIAA Guidance, Navigation, and Control Conference*, AIAA, Reston, VA, 1999, pp. 1686–1696.

[4]Kwak, S.-K., Washington, G., and Yedavalli, R. K., "Active and Passive Vibration Control of Landing Gear Components," *Proceedings of Adaptive Structures and Materials Systems*, Vol. 59, 1999, pp. 269–275.

[5]Chen, C. P., and Chopra, I., "Induced Strain Actuation of Composite Beam and Rotor Blades with Embedded Piezoceramic Elements," *Smart Structures and Materials*, Vol. 5, No. 1, 1996, pp. 35–48.

[6]Dracopoulos, T. N., and Oz, H., "Integrated Aeroelastic Control Optimization of Laminated Composite Lifting Surfaces," *Journal of Aircraft*, Vol. 29, No. 2, 1992, pp. 280–288.

[7]Fanson, J. L., and Caughey, T. K., "Positive Position Feedback Control for Large Space Structures," *AIAA Journal*, Vol. 28, No. 4, 1990, pp. 717–724.

[8]Kudva, J., Appa, K., Martin, C., and Jardine, P., "Design, Fabrication and Testing of the DARPA/WL Smart Wing Wind Tunnel Model," 38th AIAA SDM Meeting, 1997.

[9]Hustedde, C. L., Reich, G. W., Hopkins, M. A., and Griffin, K. E., "An Investigation of the Aeroelastic Tailoring for smart Structures Concept," 37th AIAA SDM Meeting, 1996.

[10]Khot, N. S., Eastep, F. E., and Kolonay, R. M., "Optimization of a Composite Wing Structure for Enhancement of the Rolling Maneuver," AIAA Paper 96-3998, 1996.

[11] Khot, N. S., Eastep, F. E., and Kolonay, R. M., "Wing Twist and Camber for the Rolling Maneuver of a Flexible Wing Without Ailerons," 38th AIAA SDM Meeting, 1997.

[12] Yedavalli, R. K., Khot, N. S., and Kwak, S. K., "Improved Aircraft Roll Maneuver Performance Using Smart Deformable Wings," *Proceedings of SPIE 5th International Symposium on Smart Structures and Materials*, Vol. 3323, Society of Photo-Optical Instrumentation Engineers, Bellingham, WA, 1998, pp. 55–66.

[13] Tseng, Y.-W., and Yedavalli, R. K., "Control Design of Linear Dynamic System with Matrix Differential Equations for Equations for Aerospace Applications," Ph.D. Dissertation, Dept. of Aerospace Engineering, The Ohio State Univ., Columbus, OH, Dec. 1997.

[14] Appa, K., and Khot, N. S., "Feasibility Assessment and Optimization Study of Smart Actuation Systems for Enhanced Aircraft Maneuver Performance," Preprint, 1997.

[15] Tzou, H. S., "Piezoelectric Shell; Distributed Sensing and Control of Continua," *Solid Mechanics and Its Applications*, Kluwer Academic, Norwell, MA, 1993, p. 19.

[16] Lee, C. K., and Moon, F. C., "Laminated Piezopolymer Plates for Torsional and Bending Sensors and Actuators," *Journal of the Acoustical Society of America*, Vol. 85, No. 6, 1989, pp. 2432–2439.

[17] Lee, C. K., "Theory of Laminated Piezoelectric Plates for the Design of Distributed Sensors/Actuators. Part I: Governing Equations and Reciprocal Relationships," *Journal of the Acoustical Society of America*, Vol. 83, No. 3, 1990, pp. 1144–1158.

[18] Lee, C. K., "Piezoelectric Laminates: Theory and Experiment for Distributed Sensors and Actuators," *Intelligent Structural Systems*, edited by H. S. Tzou, Kluwer Academic, Boston, 1992, pp. 75–167.

[19] Kwak, S. K., and Yedavalli, R. K., "New Modeling and Control Design Techniques for Aircraft Structural Dynamics Using Smart Materials," Ph.D. Dissertation, Dept. of Aerospace Engineering, The Ohio State Univ., Columbus, OH, June 1999.

[20] Ashley, H., and Zartarian, G., "Piston Theory—A New Aerodynamic Tool for the Aeroelastician," *Journal of the Aeronautical Sciences*, Vol. 23, Dec. 1956, pp. 1109–1118.

[21] Bismarck-Nasr, M. N., "Finite Element Analysis of Aeroelasticity of Plates and Shells," *Applied Mechanics Reviews*, Vol. 45, No. 12, Pt. 1, 1992, pp. 461–482.

[22] Allik, H., and Hughes, T. J. R., "Finite Element Method for Piezoelectric Vibration," *International Journal for Numerical Methods in Engineering*, Vol. 2, 1970, pp. 151–157.

[23] Tzou, H. S., and Zhong, J. P., "Electromechanics and Vibrations of Piezoelectric Shell Distributed Systems," *Transactions of the American Society of Mechanical Engineers*, Vol. 115, No. 3, 1993, pp. 506–517.

[24] Diwekar, A. M., and Yedavalli, R. K., "Smart Structure Control in Matrix Second-Order Form," *Smart Materials and Structures*, Vol. 5, No. 4, 1996, pp. 429–36.

[25] Bisplinghoff, R. L., Ashley, H., and Halfman, R. L., *Aeroelasticity*, Addison Wesley Longman, Reading, MA, 1995, p. 455.

[26] Bailey, T., and Hubbard, J. E., "Distributed Piezoelectric-Polymer Active Vibration Control of a Cantilever Beam," *Journal of Guidance, Control, and Dynamics*, Vol. 8, No. 5, 1985, pp. 605–611.

[27] Cheong, C. C., Choi, S. B., and Lee, C. H., "Position Tracking Control of a Smart Flexible Structure Featuring a Piezofilm Actuator," *Journal of Guidance, Control, and Dynamics*, Vol. 19, No. 6, 1996, pp. 1394–1369.

[28] Hanagud, H., Obal, M. W., and Calise, A. J., "Optimal Vibration Control by the use of Piezoceramic Sensors and Actuators," *Journal of Guidance, Control, and Dynamics*, Vol. 15, No. 5, 1992, pp. 1199–1206.

[29] Meirovitch, L., *Computational Methods in Structural Dynamics,* Sijthoff and Noordooff, Alphen aan den Rijn, The Netherlands, 1980, p. 62.

[30] Juang, J. N., and Phan, M., "Robust Controller Designs for Second-Order Dynamic Systems: a Virtual Passive Approach," *Journal of Guidance, Control, and Dynamics*, Vol. 15, No. 5, 1992, pp. 1192–1198.

[31] Hughes, P. C., and Skelton, R. E., "Controllability and Observability of Linear Matrix-Second-Order System," *Journal of Applied Mechanics*, Vol. 47, No. 2, 1980, pp. 415–420.

[32] Stevens, B. L., and Lewis, F. L., *Aircraft Control and Simulation*, Wiley, New York, 1992, pp. 359–376.

[33] Lewis, F. L., and Syrmos, V. L., *Optimal Control*, 2nd ed., Wiley, New York, 1995, pp. 359–375.

[34] Kirk, D. E., *Optimal Control Theory*, Prentice–Hall, Upper Saddle River, NJ, 1970, p. 93.